Morphological transition and emulsification failure in globular microemulsions

N. Shimokawa[1,a)] and S. Komura[2]
[1]*Department of Physics, Graduate School of Science, Kyoto University, Kyoto 606-8502, Japan*
[2]*Department of Chemistry, Graduate School of Science and Engineering, Tokyo Metropolitan University, Tokyo 192-0397, Japan*

(Received 17 June 2009; accepted 3 August 2009; published online 4 September 2009)

We consider the condensation transition of microemulsion droplets of oil which are dispersed in water in the presence of surfactant. Since a macroscopic oil phase is formed due to this transition, it is called "emulsification failure." Based on the free energy approach, we determine the transition lines between the spherical and the cylindrical droplet phases as well as the phase boundary lines of the emulsification failure. The phase diagrams are calculated by changing the physical properties of the surfactant monolayer such as the saddle-splay modulus and the spontaneous curvature. For a negative saddle-splay modulus, the spherical droplet phase coexists with the excess oil phase. In some cases, a re-entrant transition (sphere→cylinder→sphere) is expected to take place. For a positive saddle-splay modulus, the system undergoes a direct transition from the cylindrical droplet phase to the macroscopically phase separated state. The sphere-to-cylinder transition line approaches the emulsification failure boundary as the saddle-splay modulus becomes larger. © *2009 American Institute of Physics*. [doi:10.1063/1.3212002]

I. INTRODUCTION

Microemulsions composed of oil, water, and surfactant are thermodynamically stable fluid mixtures in which surfactant molecules adsorb at oil-water interfaces to form monolayers.[1,2] Although such mixtures appear to be homogeneous on a macroscopic length scale, the internal structure consisting of oil and water domains corresponds to a mesoscopic length scale. Hence microemulsions are considered to be a typical example of structured fluids.[3] Microemulsions are not only interesting from the viewpoint of fundamental colloid science but also useful for industrial applications such as in the preparation of foods, drugs, cosmetic products, or in the oil recovery systems. In biological systems, microemulsions are relevant to the transport of fat or to other solubilization phenomena.[4]

Various mesoscopic structures are known in microemulsions; the droplet phase where oil (water) droplets are dispersed in a continuous water (oil) region, or the bicontinuous phase where both the oil and water domains form convoluted structures in three dimensions. In the following, we consider oil-in-water (O/W) microemulsion droplet systems, but the same results apply for inverted water-in-oil (W/O) microemulsions as well. The shape of droplets can be either spherical or cylindrical depending on the composition or temperature. The structures of microemulsion droplets can be directly visualized such as using freeze fracture electron microscopy[5] or cryogenic temperature transition electron microscopy.[6]

When either the amount of oil is too large or the amount of surfactant is too small, oil droplets can contain only a limited volume of oil so that the saturated droplet phase coexists with an excess oil phase.[7–9] Such a phenomenon was later called "emulsification failure" by Safran and Turkevich.[10] As described below, they also suggested that, along the emulsification failure boundary, the droplet structure is determined by the curvature elasticity of surfactant monolayers. Various experimental techniques such as NMR self-diffusion and light scattering,[11,12] viscosity measurement,[13] small angle neutron scattering,[14] or small angle x-ray scattering[15] were used in order to identify the droplet structure near the emulsification failure boundary. All of these experiments showed that the droplets adopt a minimum size and correspond to a spherical shape. Since emulsification failure is usually unfavorable in various applications, it is important to predict the condition under which this macroscopic phase separation takes place.

From the theoretical point of view, the complex phase behavior of microemulsions has been successfully described by the Helfrich's curvature energy for flexible surfactant films.[16,17] In this model, the total free energy of a surfactant monolayer is given by

$$f_c = \sigma A + \int \mathrm{d}A \left[\frac{1}{2}\kappa(c_1 + c_2 - 2c_0)^2 + \bar{\kappa} c_1 c_2 \right], \tag{1}$$

where σ is the surface tension, A the area of the surfactant film, κ the bending modulus, $\bar{\kappa}$ the saddle-splay modulus, c_1 and c_2 the two principle curvatures, and c_0 the spontaneous curvature. Based on this curvature elasticity model, the phase diagrams of microemulsions showing various equilibrium structures such as lamellae, spheres, cylinders, or networks have been obtained.[18–22] In the work by Safran *et al.*,[18] the boundary line between the spherical droplet phase and the region of emulsification failure was determined from the condition under which the two length scales become equal.

[a)]Electronic mail: shimokawa@chem.scphys.kyoto-u.ac.jp.

The first length scale is obtained by the minimization of the above curvature energy while assuming a spherical droplet shape, i.e., $c_1=c_2=c$. Neglecting the surface tension term, this provides us with the typical length scale $1/\tilde{c}_0=(1/c_0)\times[(2\kappa+\bar{\kappa})/2\kappa]$. On the other hand, the incompressibility condition gives the second length scale $r=3a\phi_o/\phi_s$, where a is the surfactant size and ϕ_o and ϕ_s are the volume fractions of oil and surfactant, respectively. When the amount of surfactant is large so that $\tilde{c}_0 r<1$, the system is in a one-phase state forming a spherical droplet phase. However, when ϕ_s is small enough so that $\tilde{c}_0 r>1$, a certain amount of oil cannot be incorporated in the droplets and exists as an excess phase. Hence the condition for the emulsification failure is given by $\tilde{c}_0 r\approx 1$.[18]

Although the above description captures the essential feature of emulsification failure, it is not complete because neither entropy nor size distribution of the droplets are taken into account. In order to include these two effects, Sear and Cuesta[23,24] proposed a free energy formulation for spherical microemulsion droplets. In addition to oil droplets, they also considered the presence of micelles which do not contain any oil. They determined the boundary of emulsification failure according to the condition such that the total volume of oil droplets diverges. Interestingly enough, they pointed out that there is an analogy between emulsification failure and Bose–Einstein condensation.[23,24] This is because a macroscopic condensed phase is formed in both phenomena even in the absence of any interactions. It should be noted, however, that they did not consider the presence of cylindrical droplets, nor did they discuss how the phase behavior depends on the surfactant material parameters such as the saddle-splay modules or the spontaneous curvature. Another similar free energy formulation was employed in Ref. 25 which explains the closed-loop coexistence regions observed in nonionic surfactant microemulsions.

In this paper, we use the model by Sear and Cuesta in order to study the emulsification failure of both spherical and cylindrical droplet phases. Such a study is necessary because it was shown in some experiments that the excess oil phase coexists not only with the spherical droplet phase but also with either the cylindrical droplet phase or the network phase.[6,15] In addition to the emulsification failure, we also discuss the morphological transition between the spherical and the cylindrical droplet phases. We describe in detail how the phase transition lines depend on the surfactant parameters such as $\bar{\kappa}$ or c_0. We will show that the sphere-to-cylinder transition line approaches to the emulsification failure boundary as $\bar{\kappa}$ becomes larger. When $\bar{\kappa}$ is negative, the spherical droplet phase coexists with the excess oil phase. We also expect that a re-entrant transition (sphere $\rightarrow$cylinder$\rightarrow$sphere) may occur for some parameter regions. When $\bar{\kappa}$ is positive and large enough, the system undergoes a direct transition from the cylindrical droplet phase to the macroscopically phase separated state.

In Sec. II, we first discuss the model describing the emulsification failure and the morphological transition in globular microemulsions. In Sec. III, we present the results of the phase diagrams together with the free energies and the equilibrium distributions of microemulsion droplets. Some discussions and comparisons to the other works are argued in Sec. IV.

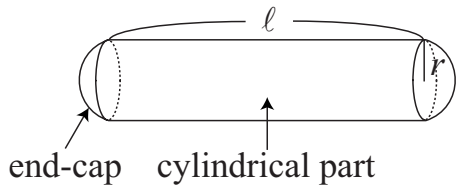

FIG. 1. Schematic representation of a cylindrical microemulsion droplet. The two end caps consist of hemispheres of radius r, and the length of the cylindrical part is ℓ. A spherical droplet corresponds to $\ell=0$.

II. MODEL

We consider O/W microemulsions where oil droplets are dispersed in water with surfactant monolayers at oil/water interfaces. We assume that the shape of oil droplets can be either spherical or cylindrical. In addition to oil droplets, we also consider the existence of spherical micelles which are composed of surfactant molecules only. The possibility of forming cylindrical micelles is excluded in the following.

In the following, all the quantities which have the dimension of length and energy are scaled by the surfactant molecular size a and the thermal energy k_BT, respectively (k_B is the Boltzmann constant and T the temperature). We denote the dimensionless volume of oil droplet by v (scaled by a^3) which can vary as $v_0\leq v\leq\infty$. For a system with the total volume V, the dimensionless free energy per unit volume F/V (measured in unit of k_BT/a^3) is given by

$$F/V=\int_{v_0}^{\infty} dv\rho(v)[\log\rho(v)-1+f(v)] + \rho_m(\log\rho_m-1+f_m), \quad (2)$$

where $\rho(v)$ is the number density of the microemulsion droplet of volume v, $f(v)$ is the internal energy of the microemulsion droplet, ρ_m is the number density of the micelle, f_m is the internal energy of the micelle. The terms $\rho(\log\rho-1)$ and $\rho_m(\log\rho_m-1)$ are the mixing entropy terms of droplets and micelles, respectively.

Next we need the expression of the internal energy f of a droplet coated by surfactant molecules. By modeling the surfactant monolayer as an elastic sheet, f can be given by the Helfrich's curvature energy f_c in Eq. (1). Hereafter, we use the notation such that σ (scaled by k_BT/a^2), κ (scaled by k_BT), $\bar{\kappa}$ (scaled by k_BT), and c_0 (scaled by $1/a$) are all dimensionless quantities. We will use the convention that the positive curvature corresponds to the case when the surfactant sheet is curved toward oil. We consider a cylindrical microemulsion droplet which consists of a cylindrical part and two hemispheres as shown in Fig. 1. The radius and the length of the cylindrical part are denoted by r and ℓ (both in unit of a), respectively. A spherical droplet corresponds to the case when $\ell=0$. Here the polydispersity in the length of the cylindrical part is not considered because it has only little effect on the phase behavior.[21] Then the internal energy of a cylindrical droplet f in Eq. (2) is given by

$$f(r) = 4\pi(\sigma + 2\kappa c_0^2)r^2 + 2\pi(\sigma\ell + 2\kappa c_0^2\ell - 8\kappa c_0)r + 4\pi(2\kappa + \bar{\kappa} - \kappa c_0\ell) + \frac{\pi\kappa\ell}{r}. \quad (3)$$

Here the variable has been changed from v to r according to the relation $v=(4\pi r^3/3)+\pi\ell r^2$. Since the radius of a spherical micelle is taken to be equal to the surfactant size a, its internal energy f_m can be obtained by setting $\ell=0$ and $r=1$ in the above equation. Then we have

$$f_m = 4\pi(\sigma + 2\kappa c_0^2) - 16\pi\kappa c_0 + 4\pi(2\kappa + \bar{\kappa}). \quad (4)$$

In microemulsions, there are two imposed constraints, i.e., both the total amount of surfactant (denoted by ξ) and the total amount of oil (denoted by ϕ) should be conserved. These conditions can be written as

$$\xi = \int_{v_0}^{\infty} dv s\rho(v) + s_m\rho_m \quad (5)$$

and

$$\phi = \int_{v_0}^{\infty} dv v\rho(v). \quad (6)$$

In Eq. (5), $s=4\pi r^2+2\pi r\ell$ and $s_m=4\pi$ are the surface areas of a microemulsion droplet and a spherical micelle, respectively.

The equilibrium distribution of microemulsion droplets can be obtained by the minimization of Eq. (2) under the constraints of Eqs. (5) and (6). This is equivalent to requiring

$$\frac{\delta}{\delta\rho}(F/V + \lambda\xi - \mu\phi) = 0, \quad (7)$$

where λ is the Lagrange multiplier and μ the chemical potential. Then we can obtain the equilibrium distribution of microemulsion droplets as

$$\rho = \exp(-f - \lambda s + \mu v). \quad (8)$$

Similarly, the equilibrium distribution of micelles is obtained by minimizing Eq. (2) with respect to ρ_m under the constraints of Eqs. (5) and (6). Then we get

$$\rho_m = \exp(-f_m - \lambda s_m). \quad (9)$$

In order to discuss the condition for emulsification failure, we look at the dependence of ϕ on v [see Eqs. (6) and (8)]. In Eq. (8), both f and s are irrelevant in the limit of $v\to\infty$ because they are proportional to r^2. Hence the distribution of droplets asymptotically behaves as $\rho\sim e^{\mu v}$ when $v\to\infty$. For $\mu\leq 0$, the distribution ρ approaches zero and ϕ takes a finite value. For $\mu>0$, on the other hand, ρ diverges so that ϕ becomes infinitely large. Notice that the case of $\phi\to\infty$ corresponds to the formation of a macroscopic oil phase, and hence the emulsification failure. Therefore the condition for emulsification failure is set by $\mu=0$.

By substituting back the equilibrium distributions of droplets ρ and micelles ρ_m into Eq. (2), we obtain the equilibrium free energy as

$$F/V = -\lambda\xi + \mu\phi - \gamma - \rho_m, \quad (10)$$

where γ is defined by

$$\gamma = \int_{v_0}^{\infty} dv\rho(v). \quad (11)$$

When the amount of oil is large enough to induce the emulsification failure, the free energy does not change any more even if the oil is further added. Then the free energy becomes

$$F/V = -\lambda_{EF}\xi - \gamma_{EF} - \rho_{mEF}, \quad (12)$$

where the subscript "EF" denotes the corresponding values at $\mu=0$. In the following calculations, the integral over the droplet volume v is replaced with the integral over the radius r by using the relation $dv=(4\pi r^2+2\pi\ell r)dr$. The integral range of r spans from 1 to ∞ since the radius of the smallest microemulsion droplet is equal to the surfactant size a. We comment that the present formulation cannot deal with nonglobular structures such as the network or the lamellar phases since the globular volume v is not well specified in these structures.

III. RESULTS

Based on the model described in Sec. II, we present the results of the free energies, phase diagrams, and equilibrium distributions of microemulsion droplets by changing $\bar{\kappa}$ and c_0 systematically. We especially pay attention to the dependence of the emulsification failure boundary and the sphere-to-cylinder transition line on the surfactant parameters or the length of cylindrical droplets. Since the obtained results qualitatively differ between negative and positive $\bar{\kappa}$, we discuss them separately.

A. Negative saddle-splay modulus ($\bar{\kappa}<0$)

Some parameters are fixed to $\sigma=0$ and $\kappa=1$ because their values do not affect the phase behavior. The others are varied as $c_0=0.1, 0.6$, $\bar{\kappa}=-0.6, -0.3$, and $\ell=0, 20, 50$. In the present formulation, the length of the cylindrical droplet ℓ cannot be determined from the minimization principle. So we regard it as a model parameter.

In Fig. 2, we show the plots of the free energy densities F/V as a function of the oil amount ϕ when the surfactant amount is fixed to $\xi=60$. In each of the graph, the solid lines are calculated from Eqs. (6) and (10) by finding the combinations of λ and μ which satisfy the fixed $\xi(=60)$ value. The dashed lines are obtained by setting $\mu=0$ at which the emulsification failure occurs. The filled circles give the crossing points between the solid and dashed lines for each ℓ. Hence they mark the onset of emulsification failure. Although not shown, each free energy curve is horizontal when ϕ exceeds the emulsification failure point. At the filled squares, the free energy of the spherical droplet crosses that of the cylindrical droplet. The possible coexistence between the spherical and cylindrical droplet phases[17,19,20] is not considered here because we are interested in how the transition lines between them are dependent on the surfactant parameters or the length of the cylindrical part. For $c_0=0.1$ [Figs. 2(a) and 2(b)], we see that the spherical droplet phase ($\ell=0$; black

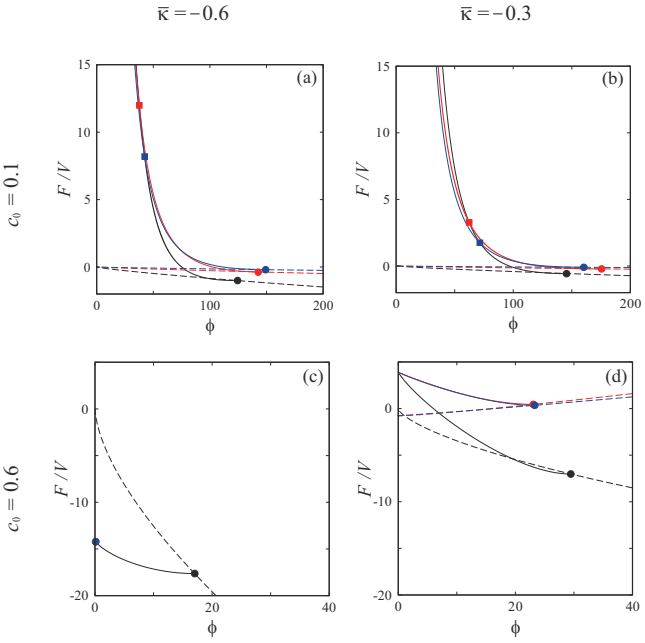

FIG. 2. Free energies per unit volume F/V as a function of the amount of oil ϕ when the amount of surfactant is $\xi=60$. The black, red, and blue solid lines indicate the free energies for $\ell=0$, 20, and 50, respectively. The dashed lines mark the emulsification failure boundary. The filled circles denote the points of emulsification failure. Although not shown, each free energy curve is horizontal when ϕ exceeds the emulsification failure point. The filled squares denote the transition points between the spherical and the cylindrical droplets. The parameters are chosen as (a) $c_0=0.1$ and $\bar{\kappa}=-0.6$, (b) $c_0=0.1$ and $\bar{\kappa}=-0.3$, (c) $c_0=0.6$ and $\bar{\kappa}=-0.6$, and (d) $c_0=0.6$ and $\bar{\kappa}=-0.3$.

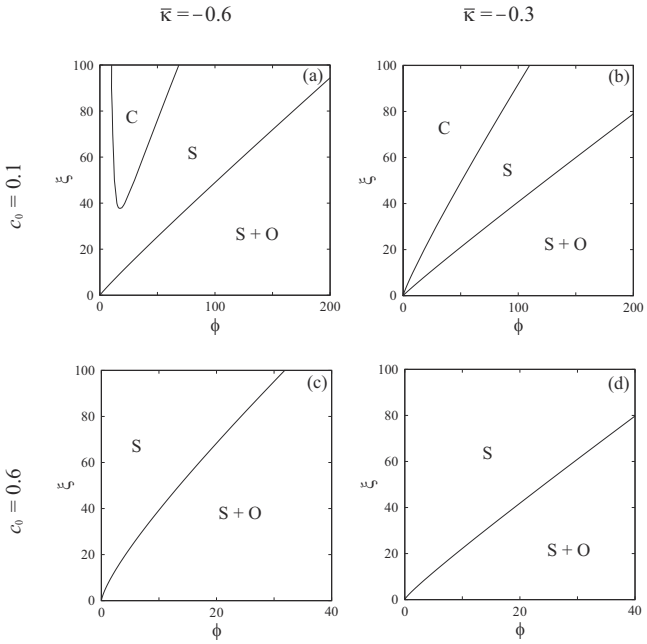

FIG. 3. Calculated boundaries of emulsification failure and phase transition lines between the spherical and the cylindrical droplet phases in the case of $\ell=20$. ϕ is the total amount of oil and ξ is the total amount of surfactant. S and C denote the spherical and the cylindrical droplet phases, respectively, while S+O indicates the coexistence between the spherical droplet phase and the excess oil. The parameters are chosen as (a) $c_0=0.1$ and $\bar{\kappa}=-0.6$, (b) $c_0=0.1$ and $\bar{\kappa}=-0.3$, (c) $c_0=0.6$ and $\bar{\kappa}=-0.6$, and (d) $c_0=0.6$ and $\bar{\kappa}=-0.3$.

lines) has the lowest energy compared to the cylindrical droplet phase ($\ell=20$; red line, or $\ell=50$; blue line) at the emulsification failure point. In these cases, the spherical droplet phase coexists with an excess oil phase. On the other hand, when ϕ is smaller than the values corresponding to the filled squares, the cylindrical droplet phase is more stable than the spherical droplet phase. Although it is not shown in Figs. 2(a) and 2(b), the spherical droplet becomes more stable again when the oil amount is made smaller than $\phi\approx 10$ ($\ell=20$).

For $c_0=0.6$ as shown in Figs. 2(c) and 2(d), the spherical droplet phase coexists with an excess oil phase similar to the case of $c_0=0.1$. However, the sphere-to-cylinder transition does not occur when $c_0=0.6$. Generally speaking, the spherical shape is energetically more favorable than the cylindrical shape when $\bar{\kappa}<0$. Moreover, since the number of cylindrical droplets for $c_0=0.6$ is much larger than that of $c_0=0.1$ (see later Fig. 5), the spherical droplet phase is far more stable. These are the reasons why the cylindrical phase does not show up here. In Fig. 2(c), even a very small amount of oil leads to the emulsification failure of the cylindrical droplet phase (hence the red and blue lines are not visible). Figure 2(d) clearly shows that the free energy of the spherical phase is always smaller than that of the cylindrical droplet phase.

These sequences of morphological transitions are summarized in Figs. 3 and 4 for $\ell=20$ and 50, respectively. We have obtained these phase diagrams by changing the value of ξ between 0 and 100. The boundary line of the emulsification failure is determined by fixing $\mu=0$ and changing λ. As the oil amount ϕ is increased from zero in Figs. 3(a) and 4(a), the spherical droplet phase (S) appears first, and it will transform to the cylindrical droplet phase (C) when ξ is large enough (such as $\xi=60$). When ϕ is further increased, the cylindrical droplet phase (C) transforms into the spherical

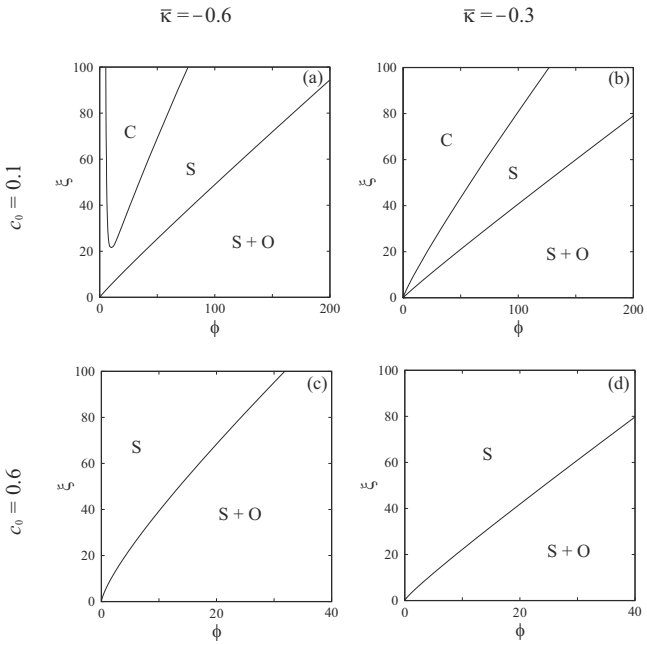

FIG. 4. Calculated boundaries of emulsification failure and phase transition lines between the spherical and the cylindrical droplet phases in the case of $\ell=50$. ϕ is the total amount of oil and ξ is the total amount of surfactant. S and C denote the spherical and the cylindrical droplet phases, respectively, while S+O indicates the coexistence between the spherical droplet phase and the excess oil. The parameters are chosen as (a) $c_0=0.1$ and $\bar{\kappa}=-0.6$, (b) $c_0=0.1$ and $\bar{\kappa}=-0.3$, (c) $c_0=0.6$ and $\bar{\kappa}=-0.6$, and (d) $c_0=0.6$ and $\bar{\kappa}=-0.3$.

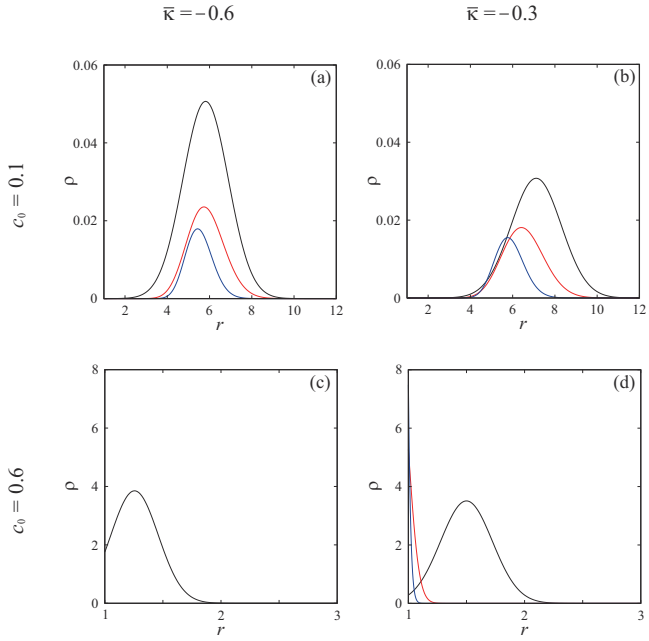

FIG. 5. Equilibrium size distribution of microemulsion droplets. r is the radius of the microemulsion droplet and ρ is its number density. The black, red, and blue lines correspond $\ell=0$, 20, and 50, respectively. The amount of surfactant is $\xi=60$. The parameters are chosen as (a) $c_0=0.1$ and $\bar{\kappa}=-0.6$, (b) $c_0=0.1$ and $\bar{\kappa}=-0.3$, (c) $c_0=0.6$ and $\bar{\kappa}=-0.6$, and (d) $c_0=0.6$ and $\bar{\kappa}=-0.3$.

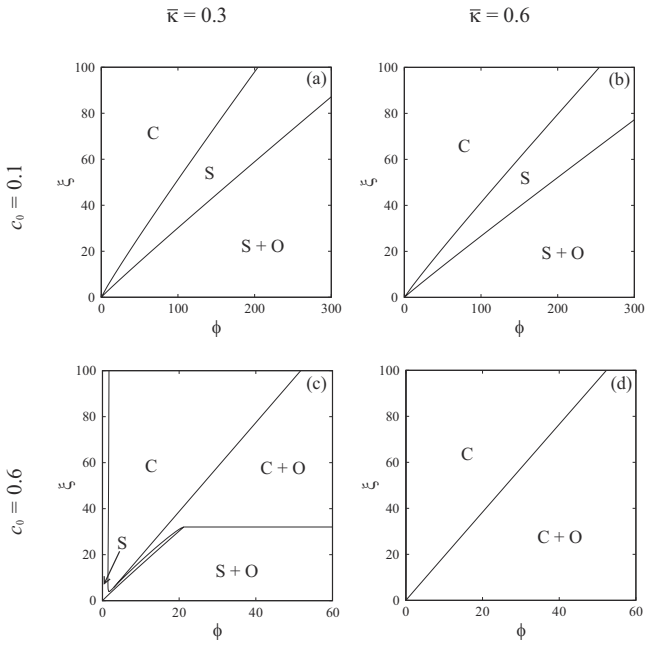

FIG. 6. Calculated boundaries of emulsification failure and phase transition lines between the spherical and cylindrical droplet phases in the case of $\ell=20$. ϕ is the total amount of oil and ξ is the total amount of surfactant. C+O indicates the coexistence between the cylindrical droplet phase and the excess oil phase, while the other notations are the same with Fig. 3. The parameters are chosen as (a) $c_0=0.1$ and $\bar{\kappa}=0.3$, (b) $c_0=0.1$ and $\bar{\kappa}=0.6$, (c) $c_0=0.6$ and $\bar{\kappa}=0.3$, and (d) $c_0=0.6$ and $\bar{\kappa}=0.6$.

droplet phase (S) again. This sequence of sphere(S) $\rightarrow$cylinder(C)$\rightarrow$sphere(S) implies a re-entrant transition. Addition of more oil results in the emulsification failure (S+O). A similar re-entrant transition exists in Figs. 3(b) and 4(b) although the region of the spherical droplet phase and the sphere-to-cylinder transition line located at $\phi\approx 0.1$ is not visible there. However, the re-entrant transition does not occur in Fig. 3(c), Fig. 3(d) Fig. 4(c), or Fig. 4(d) because the cylindrical droplet phase does not appear. [Notice that Figs. 3(c) and 3(d) are identical to Figs. 4(c) and 4(d).] We point out that, for all the phase diagrams in Figs. 3 and 4, the excess oil phase always coexists with the spherical droplet phase.

We argue next how the changes in the spontaneous curvature c_0 and/or the saddle-splay modulus $\bar{\kappa}$ affect the phase behavior. We see from Figs. 3 and 4 that the region of emulsification failure becomes smaller when either c_0 is made smaller or $\bar{\kappa}$ is made larger. The reason being that the droplet size becomes larger and the droplet phase is more stable. In other words, larger droplets can contain more oil even if the total amount of surfactant is kept the same. The sphere-to-cylinder transition line approaches the emulsification failure boundary as $\bar{\kappa}$ is increased from -0.6 to -0.3. This is because the spherical droplet phase becomes less stable as $\bar{\kappa}$ is increased. We also find that the region of the cylindrical phase for $\ell=50$ is larger than that for $\ell=20$.

Corresponding to the filled circles in Fig. 2, we show in Fig. 5 the equilibrium size distributions of droplets at the emulsification failure boundary when $\xi=60$. Different colors indicate different lengths of the cylindrical droplet. The minimum radius of a droplet is $r=1$ which is taken to be the surfactant molecular size a. Hence the droplets with $r=1$ do not contain any oil. We see that the droplet size r tends to be larger when either c_0 is made smaller or $\bar{\kappa}$ is made larger. This is consistent with the argument in Sec. I where we discussed that the optimum droplet size is given by $1/\tilde{c}_0=(1/c_0)[(2\kappa+\bar{\kappa})/2\kappa]$ for a spherical shape at the emulsifica-

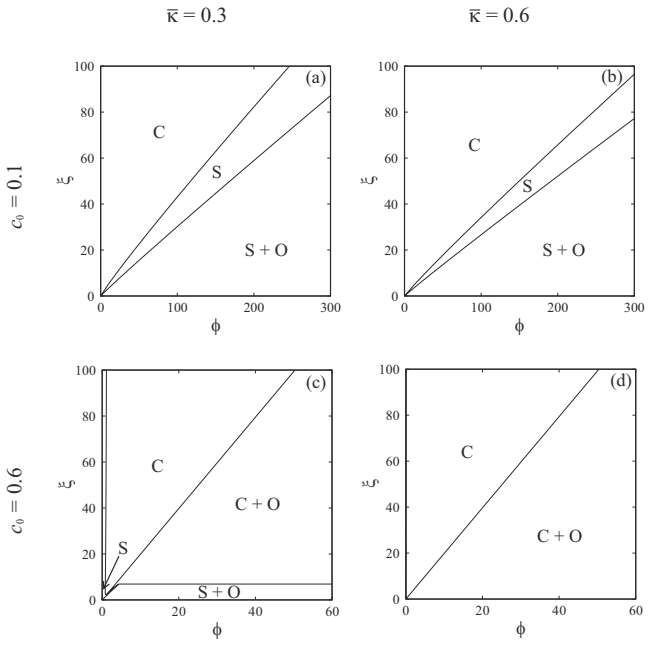

FIG. 7. Calculated boundaries of emulsification failure and phase transition lines between the spherical and the cylindrical droplet phases in the case of $\ell=50$. ϕ is the total amount of oil and ξ is the total amount of surfactant. The notations of the phases are the same with Fig. 6. The parameters are chosen as (a) $c_0=0.1$ and $\bar{\kappa}=0.3$, (b) $c_0=0.1$ and $\bar{\kappa}=0.6$, (c) $c_0=0.6$ and $\bar{\kappa}=0.3$, and (d) $c_0=0.6$ and $\bar{\kappa}=0.6$.

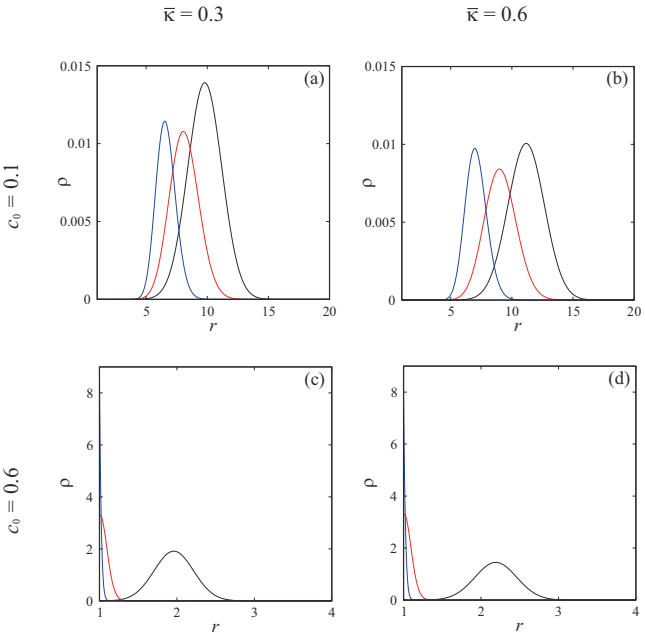

FIG. 8. Equilibrium size distribution of microemulsion droplets. r is the radius of the microemulsion droplet and ρ is its number density. The black, red, and blue lines correspond $\ell=0$, 20, and 50, respectively. The amount of surfactant is $\xi=60$. The parameters are chosen as (a) $c_0=0.1$ and $\bar{\kappa}=0.3$, (b) $c_0=0.1$ and $\bar{\kappa}=0.6$, (c) $c_0=0.6$ and $\bar{\kappa}=0.3$, and (d) $c_0=0.6$ and $\bar{\kappa}=0.6$.

tion failure boundary. We have checked that the relative peak position of the size distribution does not change appreciably even if the ξ value is varied.

B. Positive saddle-splay modulus ($\bar{\kappa}>0$)

Next we shall present the results when the saddle-splay modulus $\bar{\kappa}$ is positive. All the parameters are the same as before except $\bar{\kappa}=0.3$ and 0.6. By calculating the free energies as in Fig. 2, we obtained the phase diagrams in a similar way. In Figs. 6 and 7, we show the corresponding phase diagrams for $\ell=20$ and 50, respectively. By comparing Figs. 6(a) and 6(b), for example, we see that the region of the cylindrical phase (C) expands when $\bar{\kappa}$ is larger. Hence the sphere-to-cylinder transition line approaches the emulsification failure boundary as in the case of $\bar{\kappa}<0$. The cylindrical droplet phase coexists with the excess oil phase (C+O) for $c_0=0.6$ [see Figs. 6(c), 6(d), 7(c), and 7(d)]. Such a situation occurs when the sphere-to-cylinder transition line approaches and crosses the emulsification failure boundary line. The existence of C+O or S+O region is consistent with the experimental observation.[6]

When the surfactant amount ξ is small in Fig. 6(c), the spherical droplet phase undergoes the emulsification failure (S+O) as ϕ is increased. When ξ is large, the cylindrical droplet phase coexists with the excess oil phase (C+O). By increasing the oil amount ϕ while fixing the surfactant amount to $\xi\approx 20$, we see a rather complicated sequence of morphological transitions. First the spherical droplet phase (S) transforms into the cylindrical droplet phase (C) which undergoes the emulsification failure (C+O). As ϕ is further increased, the system exhibits the spherical droplet phase (S) which again undergoes the emulsification failure (S+O). For longer cylindrical droplets ($\ell=50$), the region of ξ which shows this complex morphological transitions becomes smaller [see Fig. 7(c)]. This kind of complex sequence of various phases is also alluded in the previous experiments.[6,7]

In Fig. 8, we show the equilibrium size distributions of the droplets at the emulsification failure boundary. Similar to the case of $\bar{\kappa}<0$, the average size is larger when $\bar{\kappa}$ is made larger and/or c_0 is made smaller. The same argument mentioned before applies here as well.

IV. DISCUSSION

Several points merit further discussion. In Figs. 3(a), 3(b), 4(a), and 4(b), we have explained that the system exhibits the re-entrant transition (sphere→cylinder→sphere) as the oil amount ϕ is increased. The mechanism of this transition can be understood as follows. In the above phase diagrams, we have shown that the spherical droplet phase is more stable than the cylindrical droplet phase when ϕ is either small or large. This is because a spherical structure is more favored when $\bar{\kappa}$ is negative. In the intermediate oil concentration, the cylindrical droplet phase appears for the following reason. We have assumed that the surfactant molecules form either monolayers or spherical micelles. In general, the formation of spherical micelles having a large curvature costs energy especially when c_0 is small. In the intermediate oil concentration, the number of created micelles associated with spherical oil droplets is larger than that associated with cylindrical oil droplets. In fact, spherical droplets need less surfactant to incorporate a fixed amount of oil so that the remaining surfactant molecules inevitably form micelles which cost high energy. As a whole, the cylindrical droplet phase can lower its energy with respect to the spherical droplet phase. It should be noted that, close to the emulsification failure boundary, almost all of the surfactant molecules are used to cover oil droplets so that micelles hardly exist.

Next we discuss why the cylindrical droplet phase undergoes a direct transition to the emulsification failure when $\bar{\kappa}>0$ [see Figs. 6(c), 6(d), 7(c), and 7(d)]. In order to understand it, we look at the size distributions of droplets given by Fig. 8(d). The peak positions are located at $r\approx 2.2$ for $\ell=0$ (spheres) or $r\approx 1$ for $\ell=20$ and 50 (cylinders). We can also check that the optimum radius obtained by the minimization of the curvature energy coincides with the corresponding peak position of the size distribution. Since most of the cylindrical droplets has $r\approx 1$, they cannot incorporate a large amount of oil. Hence the number of cylindrical droplets becomes large as seen in Fig. 8(d). Due to the same mechanism described in the previous paragraph, the cylindrical droplet phase becomes relatively stable compared with the spherical droplet phase. Moreover, cylindrical droplets are energetically favorable when $\bar{\kappa}$ is positive. According to these reasons, the cylindrical droplet phase can undergo a direct transition to the emulsification failure without changing into the spherical droplet phase.

We discuss here how our results are related to the existing experimental observations. Although many phase diagrams are explored in experimental works, it is not straightforward to compare them directly with ours because their

axes are often different. Nevertheless, some qualitative comparisons are possible. In general, the spontaneous curvature c_0 decreases as the temperature is increased. In some experiments, it was shown that the emulsification failure region becomes smaller and the droplet size becomes larger, as the temperature is increased.[6,7,13,14] The phase diagrams and the equilibrium size distributions obtained from our model exhibit the same tendencies when c_0 is decreased. On the other hand, the values of the bending modulus and the saddle-splay modulus can be deduced from interfacial tension measurements or neutron spin-echo spectroscopy.[5,26] Most of the experimental results suggest that $\bar{\kappa}$ takes a negative value so that the cylindrical droplet phase becomes more stable as c_0 is decreased. For a ternary mixture of dodecane/$C_{12}E_5$/water,[27] it was shown that the transition from the spherical droplet phase to the cylindrical droplet phase takes place as the temperature is increased. When $\bar{\kappa}<0$ (see Figs. 3 and 4), the cylindrical droplet phase does not exist in the phase diagrams for $c_0=0.6$. However, the cylindrical droplet phase becomes more stable than the spherical droplet phase as c_0 is decreased. Hence our result predicts that the transition from the sphere to cylinder may occur as the temperature is increased. This is consistent with the experimental observation.[27]

In the present theory, we treated the length of the cylindrical part ℓ as a parameter. Blokhuis and Sager[21] assumed that the polydispersity in the cylinder length obeys the Schultz distribution. This assumption is well supported by the experiment.[28] However, it was shown that the phase diagrams hardly change even if the average cylinder length is used instead of taking into account the polydispersity distribution.[21] Moreover, one of the main purposes of this paper is to reveal the dependence of the transition lines on the cylinder length. These are the reasons why we did not minimize the free energy with respect to ℓ.

Finally, we compare our results with the previous theories. Safran *et al.*[18] analyzed the relative stability among spherical, cylindrical, and planar monolayers and pointed out that the ratio $\bar{\kappa}/\kappa$ is an important parameter. While restricting only to the case of $\bar{\kappa}<0$, they showed that the sphere-to-cylinder transition approaches to the emulsification failure boundary when $\bar{\kappa}$ is increased. This is in agreement with our phase diagrams given such as in Figs. 3(a) and 3(b). They also showed that only the spherical droplet phase coexists with the excess oil phase, which is again in agreement with our result. When $\bar{\kappa}>0$, a direct transition from the cylindrical droplet phase to the emulsification failure was anticipated in Refs. 20 and 21. The corresponding phase diagram is, for example, Fig. 6(d) in our paper. We also mention that Safran *et al.* argued the coexistence between the spherical and cylindrical droplet phases,[17,19,20] and the volume fractions of sphere and cylinder in this coexistence region was calculated later in Ref. 21. However, since we are interested in the dependence of the transition lines on the surfactant parameters or the cylinder length, we did not take into account the possible phase coexistence for clarity.

V. CONCLUSION

In this paper, we have considered the emulsification failure of the microemulsion droplet phases. By taking into account both the cylindrical and the spherical droplet phases, we have obtained both the sphere-to-cylinder transition line and the emulsification failure boundary. We have discussed the effects of the saddle-splay modulus $\bar{\kappa}$ and the spontaneous curvature c_0 on the phase behavior. When $\bar{\kappa}<0$, the spherical droplet phase coexists with the excess oil phase. A re-entrant transition (sphere→cylinder→sphere) is expected for small c_0 cases. When $\bar{\kappa}>0$, a direct transition from the cylindrical droplet phase to the emulsification failure would occur as long as c_0 is large. In some case, emulsification failure may occur twice as the oil amount is increased. In general, the sphere-to-cylinder transition line approaches the emulsification failure boundary as $\bar{\kappa}$ is increased.

ACKNOWLEDGMENTS

N.S. is supported by a Japan Society for the Promotion of Science Research Fellowship for Young Scientists (Grant No. 20–10527) from the Ministry of Education, Culture, Sports, Science and Technology of Japan. S.K. thanks the support by KAKENHI (Grant-in-Aid for Scientific Research) on Priority Areas "Soft Matter Physics" and Grant No. 21540420 from the Ministry of Education, Culture, Sports, Science and Technology of Japan.

[1] G. Gompper and M. Schick, *Self-Assembling Amphiphilic Systems* (Academic, San Diego, 1994).
[2] *Micelles, Membranes, Microemulsions, and Monolayers*, edited by W. M. Gelbart, A. Ben-Shaul, and D. Roux (Springer-Verlag, New York, 1994).
[3] T. A. Witten and P. A. Pincus, *Structured Fluids: Polymers, Colloids, Surfactants* (Oxford University Press, Oxford, 2004).
[4] D. F. Evans and H. Wennerström, *The Colloidal Domain: Where Physics, Chemistry, Biology and Technology Meet* (Wiley, New York, 1999).
[5] R. Strey, Colloid Polym. Sci. **272**, 1005 (1994).
[6] A. Bernheim-Groswasser, T. Tlusty, S. A. Safran, and Y. Talmon, Langmuir **15**, 5448 (1999).
[7] H. Saito and K. Shinoda, J. Colloid Interface Sci. **24**, 10 (1967).
[8] K. Shinoda and H. Kunieda, J. Colloid Interface Sci. **42**, 381 (1973).
[9] *Micellization, Solubilization, and Microemulsions*, edited by K. W. Mittal (Plenum, New York, 1977).
[10] S. A. Safran and L. A. Turkevich, Phys. Rev. Lett. **50**, 1930 (1983).
[11] U. Olsson and P. Schurtenberger, Langmuir **9**, 3389 (1993).
[12] M. S. Leaver, U. Olsson, H. Wennerström, and R. Strey, J. Phys. II **4**, 515 (1994).
[13] M. S. Leaver and U. Olsson, Langmuir **10**, 3449 (1994).
[14] H. Bagger-Jörgensen, U. Olsson, and K. Mortensen, Langmuir **13**, 1413 (1997).
[15] J. Balogh, U. Olsson, and J. S. Pedersen, J. Dispersion Sci. Technol. **27**, 497 (2006).
[16] W. Helfrich, Z. Naturforsch **28c**, 693 (1973).
[17] S. A. Safran, *Statistical Thermodynamics of Surfaces, Interfaces and Membranes* (Addison-Wesley, Reading, 1994).
[18] S. A. Safran, L. A. Turkevich, and P. Pincus, J. Physique Lett **45**, L-69 (1984).
[19] S. A. Safran, in *Structure and Dynamics of Strongly Interacting Colloids and Supramolecular Aggregates in Solution*, edited by S. Chen, J. S. Huang, and P. Tartaglia (Kluwer Academic, Dordrecht, 1992).
[20] T. Tlusty, S. A. Safran, and R. Strey, Phys. Rev. Lett. **84**, 1244 (2000).

[21] E. M. Blokhuis and W. F. C. Sager, J. Chem. Phys. **115**, 1073 (2001).
[22] A. Zilman, S. A. Safran, T. Sottman, and R. Strey, Langmuir **20**, 2199 (2004).
[23] R. P. Sear and J. A. Cuesta, Europhys. Lett. **55**, 451 (2001).
[24] J. A. Cuesta and R. P. Sear, Phys. Rev. E **65**, 031406 (2002).
[25] R. Menes, S. A. Safran, and R. Strey, Phys. Rev. Lett. **74**, 3399 (1995).
[26] T. Hellweg and D. Langevin, Phys. Rev. E **57**, 6825 (1998).
[27] T. Hellweg and R. von Klitzing, Physica A **283**, 349 (2000).
[28] D. I. Svergun, P. V. Konarev, V. V. Volkov, M. H. J. Koch, W. F. C. Sager, J. Smeets, and E. M. Blokhuis, J. Chem. Phys. **113**, 1651 (2000).